Near-Field Dynamics of Diesel and Biodiesel Sprays at 200 MPa Injection Pressure

S. MOON
National Institute of Advanced Industrial Science and Technology, Tsukuba, JAPAN
ss.moon@aist.go.jp

X. ZHANG, Y. GAO, J. WANG*
Argonne National Laboratory, Argonne, IL, US
xzhang@aps.anl.gov, ygao@aps.anl.gov, wangj@aps.anl.gov

T. TSUJIMURA
National Institute of Advanced Industrial Science and Technology, Tsukuba, JAPAN
tsujimura-taku@aist.go.jp

N. KURIMOTO, Y. NISHIJIMA
DENSO CORPORATION, Kariya, JAPAN
NAOKI_KURIMOTO@denso.co.jp, YOSHIAKI_NISHIJIMA@denso.co.jp

Abstract

High-pressure, high-speed diesel fuel sprays are complex multiphase flow phenomena. Great efforts have been devoted to understand their dynamics that is essential to the breakup, especially, in this near-nozzle region. However, conventional optical techniques are not effective to probe the dynamics in the first several millimeters of the optically dense region, where liquid is fast and in a complex morphology. By taking advantage of high-intensity and high-brilliance x-ray beams available at the Advanced Photon Source (APS), the morphology of the sprays can be imaged with ultrafast x-ray micro-imaging techniques and with sub-ns temporal resolution.

Furthermore, two short x-ray pulses (sub-nanosecond to a few nanoseconds) with a variety of intervals can be used to visualize the high-speed sprays. By tracking the movement of features in the double-exposure images without the need of seed particles, it becomes well possible to derive velocity fields of the sprays in the near-nozzle region. To understand near-field flow dynamics of diesel and biodiesel sprays injected at 200 MPa and travelling at a velocity exceeding 600 m/s, double-exposed images were taken using x-ray pulses with time interval of 68 ns. By using auto-correlation analysis, the near-field spray velocity can be obtained quantitatively.

We recorded the double-exposed x-ray images and derived auto-correlation functions of diesel and biodiesel sprays under various injection pressures up to 200 MPa. We note that 200 MPa injection pressure is not the maximum limit for the x-ray method rather it was limited by the specification of the fuel-injection system. The theoretical velocity was calculated using Bernoulli equation, which was compared against measurement. The results showed that the axial velocity increased with increase in injection pressure and reached over 600 m/s at 200 MPa injection pressure. We also made comparison between diesel and biodiesel sprays under various injection pressures. To probe the interaction between the sprays and surrounding gas, the local flow velocities were measured at different axial and radial locations. The results will prove valuable in providing validation of internal-flow and spray modeling.

Introduction

Recent research trend in internal combustion engines is highly oriented to direct-injection (DI) diesel engines which normally guarantee higher thermodynamic efficiency and lower carbon-dioxide (CO_2) emissions than conventional gasoline engines **[1]**. During last decade, the injection pressures applied for DI diesel engines kept increasing to achieve faster atomization and mixing with oxidant gas and to accomplish corresponding clean and efficient combustion **[2, 3]**. In the mean time, due to environmental issues and upcoming depletion of fossil fuels, the new-type diesel fuel derived by biological resources (biodiesel) has been applied to commercial diesel engines as a form of mixture with diesel fuel **[4]**.

Considerable researches have been performed to understand the spraying process of high-pressure diesel sprays which initiates ignition and governs flame propagation and chemical reaction during the combustion

* Corresponding author: wangj@aps.anl.gov

process. Tons of database have been collected for interpertation of spraying process and these have contributed for improvement and optimization of DI diesel engines **[1, 5]**. Nevertheless, concrete understanding on near-field flow dynamics, which is valuable in accurate modeling of inter-nozzle flow and spraying process, has not been made so far. Conventional optical techniques are not effective to probe the dynamics in the first several millimeters of the optically dense region, where fuel liquid is in supersonic speed and in a complex morphology. Some analytical models have been proposed and adopted for considerable modeling works **[6-10]**, but their validation has been made indirectly through macroscopic or microscopic spray information at farther downstream due to lack of information on near-field dynamics and breakup process. Especially for new biofuels, application of conventional models should be carefully validated, since their physical properties and chemical compositions are quite different with those of conventional diesel fuel.

By taking advantage of high-intensity and high-brilliance x-ray beams available at the Advanced Photon Source (APS), the morphology of the high-pressure diesel sprays can be imaged in the near-field with ultrafast x-ray phase-enhanced imaging techniques and with sub-ns temporal resolution [**11-12**]. Furthermore, two short x-ray pulses (sub-nanosecond to a few nanoseconds) with a variety of intervals can be used to visualize the high-speed sprays. By tracking the movement of features in the double-exposure images without the need of seed particles, it becomes well possible to derive velocity fields of the sprays in the near-nozzle region. A previous study utilized this advantage of x-ray beams for analysis of near-field dynamics of single- and dual-hole nozzle gasoline sprays injected with 2 MPa injection pressure [**13**]. Double exposed x-ray micro-images were recorded and the velocities were obtained through autocorrelation analysis (structure-tracking velocimetry). This pioneering study successfully analyzed the near-field spray velocity at the range of 20 to 60 m/s. However, application of this technique is not extended to the diesel sprays which are in supersonic speed and optically dense in the near-field.

In this study, we apply the structure-tracking velocimetry technique to supersonic diesel and biodiesel sprays and discuss the reliability of the results. Then we analyze local velocity distribution of diesel and biodiesel sprays with up to 200 MPa injection pressure to investigate the effect of injection conditions and fuels on near-field dynamics. The double-exposed images were taken using x-ray pulses with time interval of 68 ns to trace the structures in the supersonic sprays. Autocorrelation analysis is performed for the double-exposed images for calculation of near-field local spray velocity quantitatively.

Experiments

The experiments were performed using a x-ray phase-enhanced imaging setup at XOR 7ID beamline in the APS, shown in Fig. 1a. The x-ray beam was generated from an insertion device (undulator) in the APS electron storage ring. The special beam pattern (hybrid-singlet mode) shown in Fig. 1b was used in this experiment. This pattern contains a single electron bunch (150 ps duration, 16 mA current) isolated from the remaining electron train bunch containing 8 pulses (472 ns long, periodicity of 68 ns, 11mA current for each pulse) by symmetrical 1.594 μs gaps. The single electron bunch was used for single-exposed imaging and the two pulses of the remaining train bunch were used for double-exposed imaging (refer Fig. 1b). To reduce the heat power, the x-ray beam was chopped by two mechanical shutters: the slow shutter operating at 1Hz frequency with 8 ms opening duration and the fast shutter operating at 1 kHz frequency with 9 μs opening duration. Synchronized operation of these two shutters cuts-off more than 99% of the beam heat power.

After transmitted to the spray, the x-ray beam generates the phase-enhanced image on a scintillator crystal (LYSO:Ce), which converts the transmitted x-ray beam into visible light (432 nm). This image is reflected by a 45^{o} mirror and then captured by a charge-coupled device (CCD) camera (Sensicam, 1376×1040 pixels, from Cooke). The field of view of the camera was 1.74×1.32 mm^2 and the image resolution was 1.26μm/pixel when a 5x objective lens was used.

The fuel was injected into a spray chamber using a common-rail injection system, composed of fuel tank, motor, high-pressure pump, pressure valve and common-rail. The pressure inside the common rail was controlled via feedback control of measured pressure inside the common-rail and bleeding fuel flow rate of the pressure valve. The spray chamber has two Kapton windows which allow the x-ray beam to pass through these without decrease in intensity.

Table 1 shows the experimental conditions. A single-hole nozzle, which orifice diameter (D) is 0.120 mm and discharge coefficient (ratio of actual flow rate to ideal flow rate; C_d) is 0.88, was used as the test nozzle. The applied injection pressures were ranged from 50 MPa to 200 MPa. A biodiesel and a diesel fuel were used as the test fuels in this study to investigate the effect of fuel properties on near-field dynamics. Biodiesel has higher density, viscosity and surface tension than the diesel fuel. A gentle nitrogen (N_2) flow was supplied to the spray chamber to blow out the injected fuel. The sprays were injected into the surroundings in atmospheric pressure and room temperature conditions. Applied injection pulse duration was 1ms. From the preliminary test, it was found that the spray reaches its steady state over 100 μm needle lift and the needle reaches its top location at 1ms

after the start of injection (aSOI) regardless of the injection pressures. Since this study focuses on the near-field dynamics at steady-state, all of spray images were taken at 1 ms aSOI.

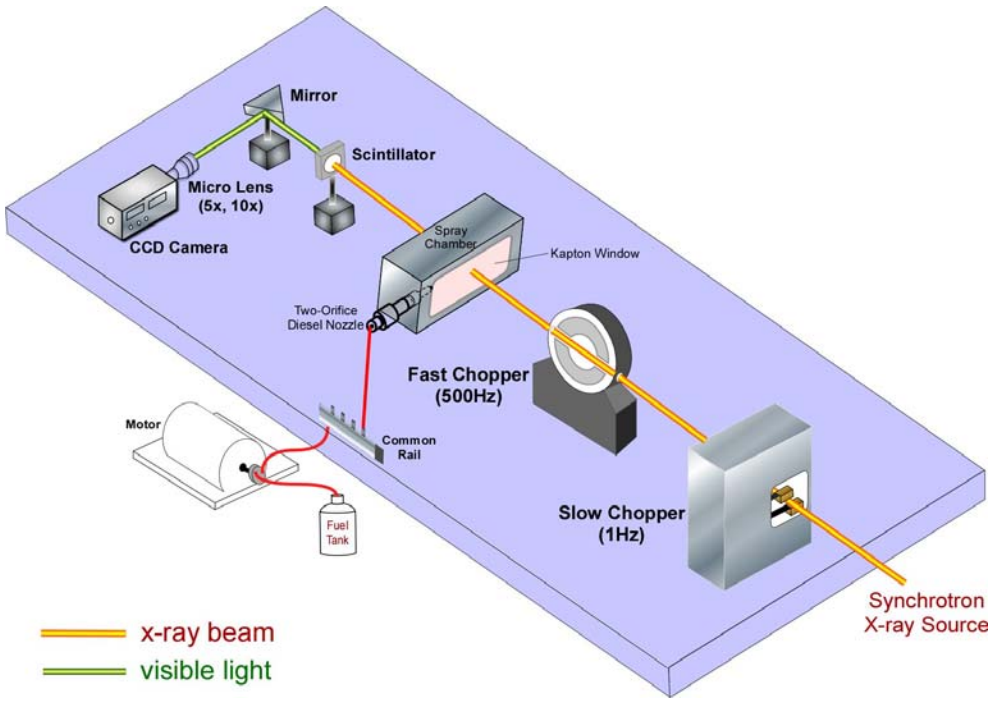

(a)

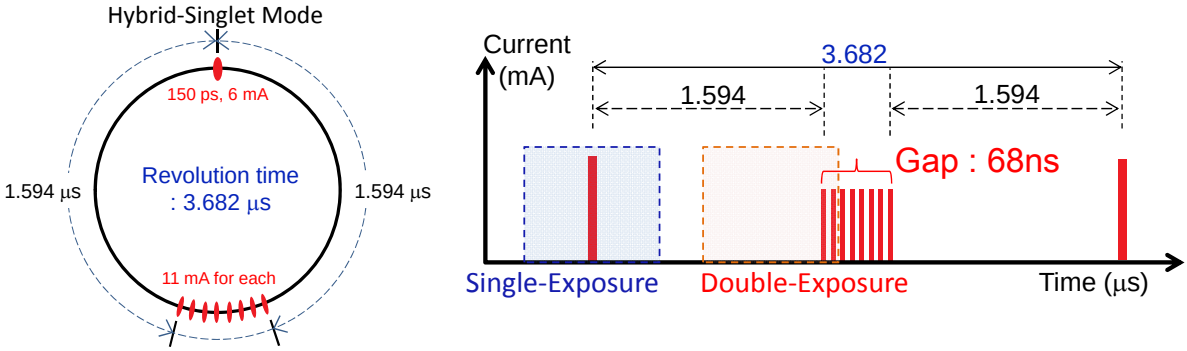

(b)

Fig. 1 Experimental setup (a) and beam pattern (b) for single- and double-exposed x-ray phase-enhanced Imaging

Table 1 Experimental Conditions

Nozzle	Single-Hole Nozzle (D=0.120mm, C_d=0.88)			
Injection Pressure (P_{inj})	50, 100, 150, 200 MPa			
Injection Duration (T_{inj})	1.0 ms			
Ambient Pressure	Atmospheric			
Ambient Temperature	Room Condition (300 K)			
Ambient gas	Nitrogen (N_2)			
Fuel		Density (kg/m^3)	Kinematic Viscosity (mm^2/s)	Surface Tension (N/m)
	Biodiesel	849.9	6.10	0.032
	Diesel	835.2	3.32	0.026

Results and Discussion

Auto-correlation Analysis of Double-Exposed Images

In this section, we carefully discuss the reliability of the velocity results obtained by auto-correlation analysis of double-exposed x-ray phase-enhanced images. X-ray phase-enhanced images have the line-of-sight nature and show phase variations of the emerging radiation from liquid/gas interfaces rather than absorption-induced intensity variations when the x-ray beam passes through an object [**14**]. In the previous studies, it has been found that the features smaller than 10 μm are hard to be detected from the phase-enhanced images. Therefore, we here note that the morphologies in the phase-enhanced images show the features overlapped through the beam path and larger than 10μm.The left-side images in Fig. 2 show the double-exposed x-ray phase-enhanced images of diesel sprays at 5 mm axial distance with 100 and 200 MPa injection pressures. The duplicated features by double-exposure can be clearly seen in the images. In spray studies, cross-correlation method is generally used to calculate the flow or ambient gas velocity using two individual images taken with very short time interval [**15-17**]. In this method, after defining the base interrogation window for two images at same location, the grayscale correlation factor which shows the similarity between two images are calculated with shifting the interrogation window of the second-captured image. The shifted quantity of interrogation window at maximum correlation factor represents the most probable displacement of the flow during the time interval. Equation 1 shows the grayscale correlation factor (*C*) generally applied for the cross-correlation method.

$$C = \frac{\sum_m \sum_n (A(m,n) - \overline{A})(B(m,n) - \overline{B})}{\sqrt{\left(\sum_m \sum_n (A(m,n) - \overline{A})^2\right)\left(\sum_m \sum_n (B(m,n) - \overline{B})^2\right)}} \quad (1)$$

where, *A* and *B* are the integration windows of first- and second-captured images respectively, and $\overline{A}$ and $\overline{B}$ are the mean intensity of the interrogation windows.

The concept of auto-correlation is identical with cross-correlation, but only difference is that we use single image containing duplicated features for self-correlation other than using two individual images. Considering that the morphologies in the spray themselves have certain frequencies, cross-correlation can be a better way for structure-tracking. The reason we applied auto-correlation in this study instead of cross-correlation is that performances of current cameras are not feasible to take two individual shots with this short time interval (68 ns). The results of 30-shot averaged correlation factor contours with the interrogation window of the dotted box are shown in right-side of Fig. 2. The auto-correlation results showed quite clear contour and symmetric peaks of the correlation factors for both injection pressures.

There are some issues should be carefully considered to obtain reliable velocity results from auto-correlation analysis of double-exposed images. First, we need to confirm whether the peaks in the correlation factor contours are from the duplicated features from double-exposure or not. To confirm this, auto-correlation was performed for single-exposure images and the results were compared to those of double-exposure images. The results showed that the single-exposure images do not show clear peaks in the correlation factor contours, indicating that the peaks in Fig. 2 are from double-exposed features in the spray.

Second, we need to carefully consider the line-of-sight nature of the phase-enhanced images. As aforementioned, the phase-contrast images contain all of flow information through the beam path. Hence, the spray center of the image in Fig. 3 (R=0) would contain all of flow displacements from the spray center to the periphery (R=0-189 μm). The profiles of 30-shot averaged correlation factors along the line connecting two peaks of correlation factor contour at different radial locations (R) are shown in Fig. 3. At the spray periphery (R=189 μm), the correlation factor profile was relatively sharper than that at smaller R regions because the morphologies are less concentrated and less overlapped through the beam path (refer the schematic in Fig. 3). As approaching to the central region of the spray, the correlation factor profiles get less sharp and stretched horizontally indicating that the flow displacements of outer regions are somehow smeared in this profile. Nevertheless, the location of displacement peak (DP) gets farther from the contour center which well follows a general understanding that the spray velocity increases as approaching to the spray center. Regarding that the velocity at a certain R location should be higher than that at outer R regions, the results in Fig. 3 show that the DP of the correlation factor contour is dominated by the flow displacement at that local location rather than that at outer regions. Reconstruction of velocity results would be the best way to obtain reliable local velocity from line-of-sight images, but it is hard to be implemented so far. To further confirm the reliability of the velocity results, the velocity coefficient (ratio of actual velocity to the ideal velocity) calculated from the velocity results was compared to the C_d obtained by the flow measurement. The results from two methods were quite consistent with only around 2% difference. Because no hydraulic flip was observed in the phase-enhanced images (not included), it therefore confirms that the velocity results are quite reliable.

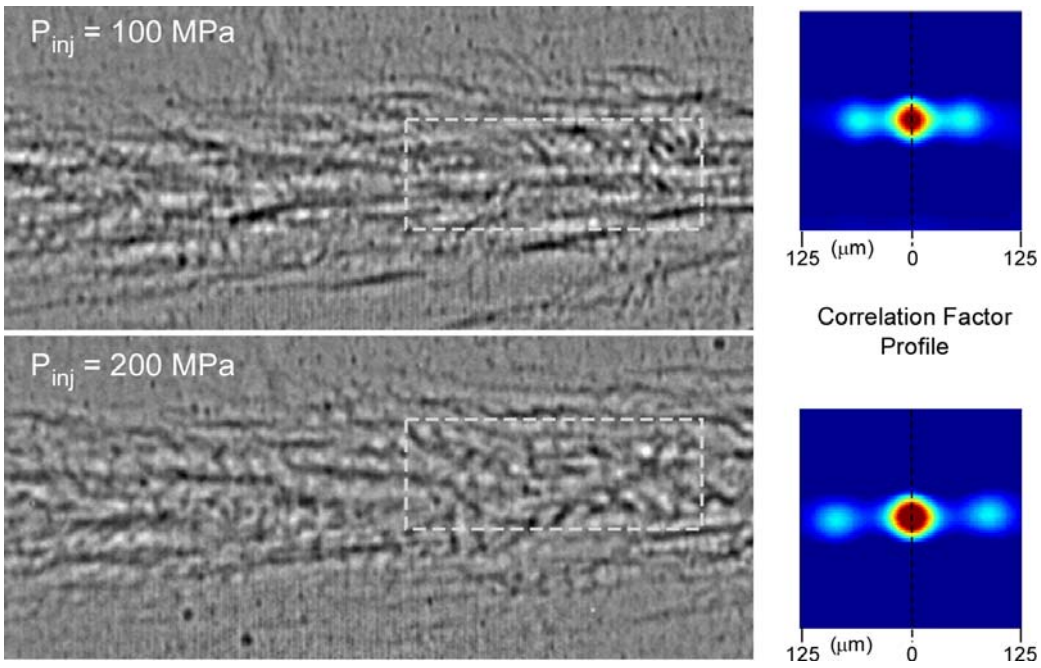

Fig. 2 Double-exposed phase-enhanced images and correlation factor contours at 100 MPa and 200 MPa injection pressures; diesel, steady-state, axial distance (x)=5 mm location

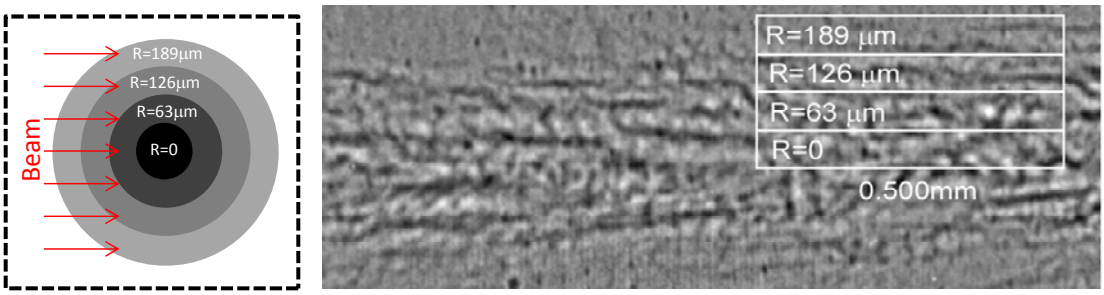

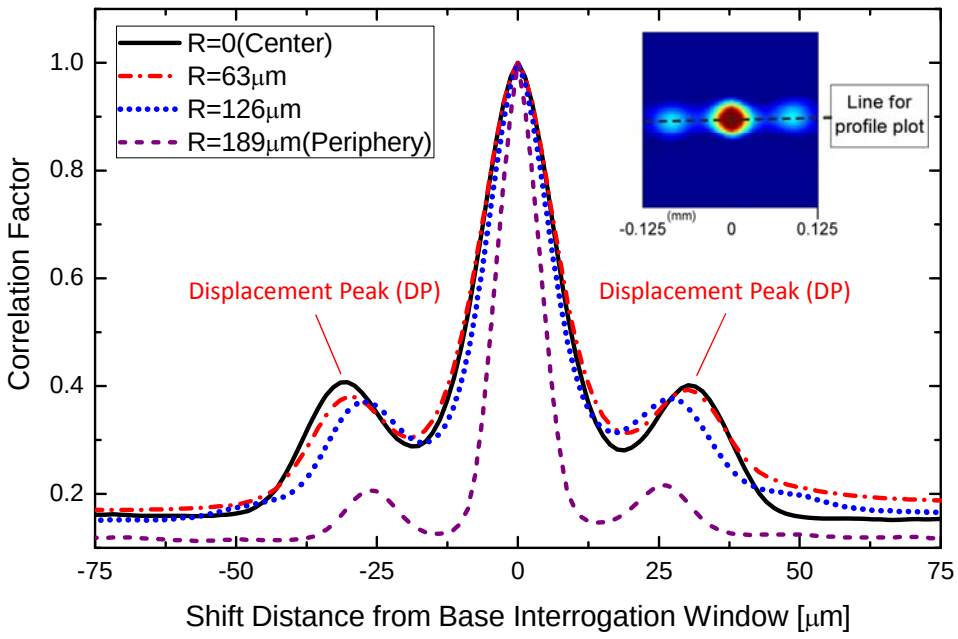

Fig. 3 Correlation factor profiles at various radial locations; P_{inj}=100 MPa; diesel, steady-state, x=5 mm location

Flow Discharge Performance

Figure 4 shows the axial velocity and velocity coefficient (C_v) of the sprays at 5mm distance to discuss the flow discharge characteristics at different injection conditions. The velocities were calculated by dividing the location of DP by time gap between two pulses (68ns). Biodiesel sprays at low injection pressures do not have clear flow features to track until 5 mm distance supposedly due to their high viscosity, comparison and discussion are made at 5 mm location. The flow discharge is generally discussed with the discharge coefficient (C_d) in spray studies. The velocity coefficient (C_v) was, however, used instead in this study, since it was hard to integrate the flow rate using the local velocity results. The C_v was defined as the ratio of actual flow velocity to ideal flow velocity (V_{actual} / V_{ideal}) and the ideal velocity was calculated using Bernoulli equation.

As expected, the axial velocity increased with increase in injection pressure and reached over 600 m/s (Ma 2) at 200 MPa injection pressure. However, the fuel properties did not play a significant role in the axial velocity. Up to 100 MPa injection pressure, the flow discharge of biodiesel spray was almost identical with that of diesel spray, while it showed slight decrease at higher injection pressures. The C_v was almost independent to the injection pressure and fuels and it was around 0.86. This value is quite similar to the C_d measured by experiment (0.88).

Local Velocity Distribution and Spray/Air Interaction

Another interesting topic can be discussed here is local velocity distribution of the sprays that is important to understand how the sprays interact with surrounding air in the near-field.

Figure 5a shows the radial velocity distribution of the diesel sprays at three axial locations with the injection pressures of 100 MPa and 200 MPa. The 30-shot averaged velocity results and its shot-to-shot deviations are plotted. For both injection pressures, at the nozzle exit (x=1 mm), the velocity at the radial location of 63 μm was smaller than that at the spray center. This radial velocity profile at the nozzle exit seems induced by inter-nozzle flow affected by boundary layer other than spray/air interaction. At downstream, the velocity at the spray center remained same until 5mm location for both injection pressures, while the velocity at the spray peripheries decreased distinctively with axial distance. It indicates that the aerodynamic effect is minor at the spray center but dominant at the spray peripheries in the near field. It also indicates that the self-similarity of the spray is not applicable in the near-field. At 200 MPa injection pressure, decrease of local velocity at spray periphery with increase in axial distance was higher than that at 100 MPa. It tells that the aerodynamic effect plays more significant role at higher injection pressures due to higher relative velocity between spray and surrounding air. The shot-to-shot deviation of the velocity at the spray peripheries increased with increase in axial distance and at 200MPa injection pressure indicating that the flows are more turbulent at downstream and at high injection pressures.

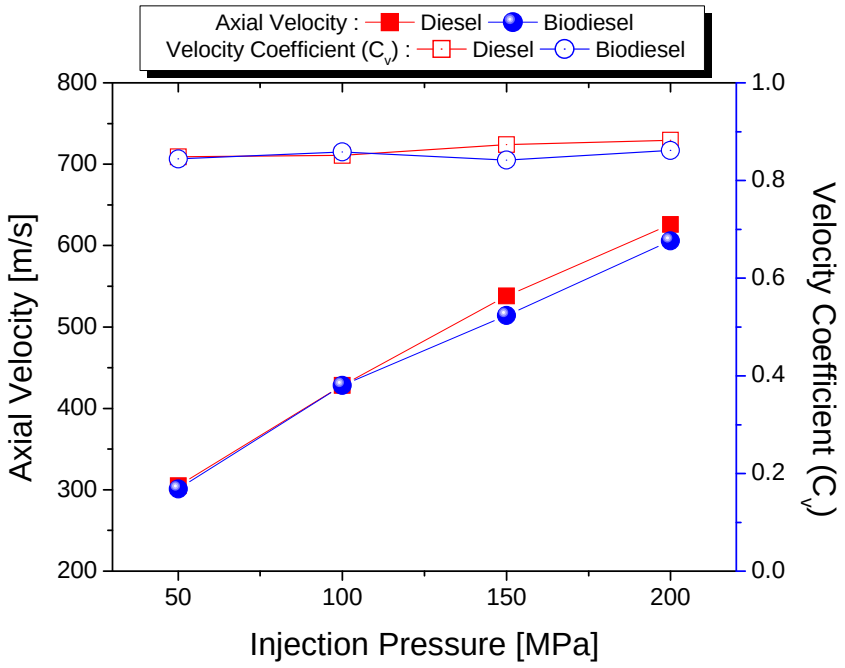

Fig. 4 Axial velocity of diesel and biodiesel sprays at different injection pressures; steady-state, x=5 mm location

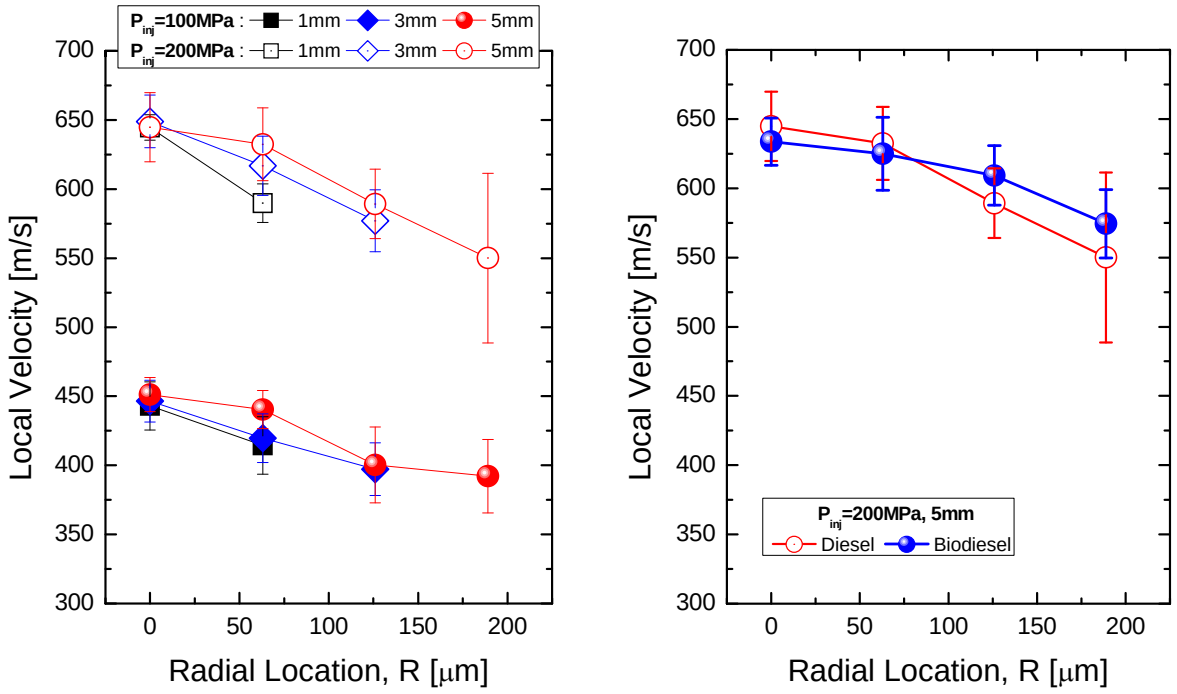

(a) (b)

Fig. 5 Local velocity distribution at different injection pressures and fuels; steady-state, (a) Effect of injection pressure, (b) Effect of fuel

Comparison of local velocity distribution of diesel and biodiesel sprays is presented in Fig. 5b. As aforementioned, because the biodiesel spray does not have clear features to trace near the nozzle exit, the comparison of local velocity is made at 5 mm distance with 200 MPa injection pressure. As shown in Fig. 4, the biodiesel spray has lower velocity than diesel spray at the spray center. Decrease rate of spray velocity with increase in radial distance appeared smaller for biodiesel spray indicating that the high viscosity biodiesel spray has less turbulent flow in the near-field and less active spray/air interaction at the spray periphery. Smaller shot-to-shot deviation of the biodiesel spray at all radial locations supports this explanation.

Summary and Conclusions

In this study, near-field dynamics of supersonic diesel and biodiesel sprays are discussed up to 200 MPa injection pressures using auto-correlation analysis of double-exposed x-ray phase-enhanced images. To obtain double-exposed images of the supersonic sprays, two x-ray pulses with pulse gap of 68 ns were used in this study. Methodology, reliability and limitations of the auto-correlation analysis for calculation of local velocity are carefully considered. From the local velocity results, characteristics of flow discharge and spray/air interaction in the near-field under various injection conditions are discussed. The main findings from this study are summarized below.

- Auto-correlation analysis of double-exposed x-ray phase-enhanced images showed reliable local velocity results of the supersonic sprays, nevertheless the line-of-sight nature of the x-ray phase enhanced-images. Reliability of the velocity results was confirmed by comparing the velocity coefficient (ratio of actual velocity to ideal velocity) obtained by auto-correlation analysis to the discharge coefficient (ratio of actual flow rate to ideal flow rate) measured by experiment.
- The spray center velocity increased with increase in injection pressure and it reached over 600 m/s (Ma 2) at 200 MPa injection pressure. The spray center velocity was almost independent to the fuels, but biodiesel sprays showed slightly lower center velocity (3~5%) compared to diesel spray at over 100 MPa injection pressures. The velocity coefficient (flow discharge performance) was almost independent to injection pressures and fuels applied in this study.
- The local velocity distribution was quite dependent to the injection pressures and fuels. While the axial velocity did not show any decrease until 5 mm distance, the velocity at the spray periphery decreased distinctively with axial distance. Decrease rate of local velocity with axial distance and shot-to-shot deviation at the spray periphery increased at higher injection pressures indicating that spray/air interaction is more ac-

tive and the flow is more turbulent at high injection pressures. The biodiesel spray showed less turbulent and less active spray/air interaction compared to the diesel spray.

In the following studies, the flow dynamics will be analyzed from nozzle exit to further downstream to investigate the start location of velocity decay (intact core length), velocity decay rate with axial distance and self-similarity of the spray at different injection conditions. We expect these will provide clear view and understanding on initial spray/air mixing process and related ignition and flame lift-off characteristics at different injection conditions.

Acknowledgements

This work and the use of the APS were supported by US Department of Energy (DOE), Office of Science/Basic Energy Science and Energy Efficiency and Renewable Energy/Vehicle Technology. This work was also supported by Ministry of Economy, Industry, and Trade (METI) Japan as a part of Japan-U.S. cooperation project for research and standardization of Clean Energy Technologies. The authors thank the financial support from DOE in US and METI in Japan.

References

[1] Heywood, J. B., Internal combustion engine fundamentals, McGraw-Hill, 1988.
[2] Dodge, L. G., Simescu, S., Neely, G. D., SAE Paper 2002-01-0494 (2002)
[3] Wang, X., Huang, Z., Zhang, W., Kuti, O. A., Nishida, K., *Applied Energy* 88: 1620-1628 (2011)
[4] Lapuerta, M., Armas, O., Rodriguez-Fernandez, J., *Progress in Energy and Combustion Science* 34: 198-223 (2008)
[5] Naber, J. D., Siebers D. L., SAE Paper 960034 (1996)
[6] Taylor, G. I., *The Scientific Papers of G. I. Taylor 3*: 244-254 (1963)
[7] Reitz, R. D., Bracco, F. V., *Physics of Fluids* 25, 1730-1742 (1983)
[8] Reitz, R. D., Bracco, F. V., *Encyclopedia of Fluid Mechanics* 3, Chapter 10 (1983)
[9] Spalding, D. B., Combustion and mass transfer, Pergamon Press (1979)
[10] Densantes, J. M., Payri, R., Salvador, F. J., Gil, A., *Fuel* 85: 910-917 (2006)
[11] Lai, M. –C., Zheng, Y., Xie, X., Moon, S., Liu, Z., Gao, J., Zhang, X., Fezzaa, K., Wang, J., and Shi, J., SAE Paper 2011-01-0681 (2011)
[12] Wang, Y., Im, K., and Fezzaa, K., *Physical Review Letters* 100:154502 (2008)
[13] Wang, Y., Liu, X., Im, K., Lee, W. –K., Wang, J., Fezzaa, K., Hung, D. L. S., and Winkleman, *Nature Physics* 4:305-309 (2008)
[14] Wilkins, S. W., Gureyev, T. E., Gao, D., Pogany, A., and Stevenson, A. W., *Letters to Nature* 384:335-338 (1996).
[15] Andrian, R. J., *Applied Optics* 23: 1690-1691 (1984)
[16] Willert, C. E., Gharib, M., *Experiments in Fluids* 10: 181-193 (1991)
[17] Moon, S., Matsumoto, Y., Nishida, K., Gao, J., *Fuel* 89: 3287-3299 (2010)